Available online at www.sciencedirect.com

ScienceDirect

journal homepage: www.elsevier.com/locate/he

Low-temperature partial oxidation of methane over Pd–Ni bimetallic catalysts supported on CeO_2

Shiva Fazlikeshteli, Xavier Vendrell[**], *Jordi Llorca*[*]

Institute of Energy Technologies, Department of Chemical Engineering and Barcelona Research Center in Multiscale Science and Engineering, Universitat Politècnica de Catalunya, EEBE, Eduard Maristany 16, 08019, Barcelona, Spain

HIGHLIGHTS

- Bimetallic Pd–Ni/CeO_2 prepared by ball milling show excellent performance for POM.
- Maximum methane conversion and syngas with 0.12 wt% Pd and 1.38 wt% Ni.
- Superior stability for Pd–Ni/CeO_2 ball milled at 50 Hz for 20 min.
- Ball milling yields an impressive dispersion of metal species on CeO_2 surface.

GRAPHICAL ABSTRACT

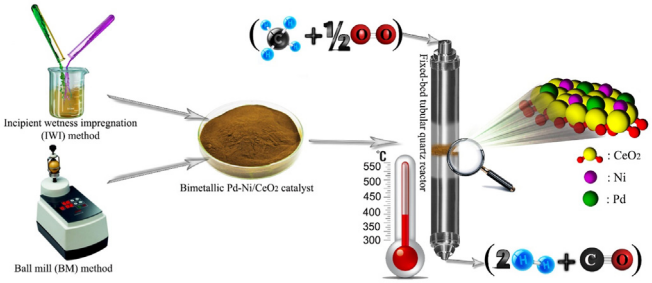

ARTICLE INFO

Article history:
Received 1 February 2022
Received in revised form
26 June 2022
Accepted 3 July 2022
Available online 13 August 2022

Keywords:
Methane partial oxidation
Bimetallic catalysts
Ceria catalysts
Palladium
Nickel
Mechanochemistry

ABSTRACT

Monometallic Pd and Ni and bimetallic Pd–Ni catalysts supported on CeO_2 are prepared via mechanochemical and conventional incipient wetness impregnation methods and tested for the production of syngas by the partial oxidation of methane. Compared with monometallic Ni/CeO_2 and Pd/CeO_2, bimetallic Pd–Ni/CeO_2 catalysts show considerable higher methane conversion and syngas yield. Additionally, the bimetallic catalysts prepared by ball milling produce syngas at lower temperature. Different preparation parameters, such as metal loading, Pd/Ni ratio, milling energy, milling time and order of incorporation of the metals are examined. The best performance is obtained with a bimetallic catalyst prepared at 50 Hz for 20 min with only 0.12 wt% Pd and 1.38 wt% Ni. Stability tests demonstrate superior stability for bimetallic Pd–Ni/CeO_2 catalysts prepared by a mechanochemical approach. From the characterization results, this is explained in terms of an impressive dispersion of metal species with a strong interaction with the surface of CeO_2.

* *Corresponding author.*
** *Corresponding author.*
E-mail addresses: xavier.vendrell.villafruela@upc.edu (X. Vendrell), jordi.llorca@upc.edu (J. Llorca).

https://doi.org/10.1016/j.ijhydene.2022.07.020

Introduction

Methane is a major component of natural gas (>90%) and its conversion into syngas (a valuable feedstock composed by a mixture of gases dominated by the presence of carbon monoxide CO and hydrogen) has attracted increasing attention in the last few decades for the production of numerous chemical products and fuels [1–3]. Depending on the application, the catalytic syngas production from methane can be realized through three general routes: (1) steam reforming of methane (SRM) (Eq. (1)), (2) dry reforming of methane (DRM) (Eq. (2)), and (3) partial oxidation of methane (POM) (Eq. (3)) [4–6].

$$CH_4 + H_2O \longrightarrow CO + 3H_2 \qquad \Delta H_{298K} = 206\ kJ\ mol^{-1} \qquad (Eq.\ 1)$$

$$CH_4 + CO_2 \longrightarrow 2H_2 + 2CO \qquad \Delta H_{298K} = 247\ kJ\ mol^{-1} \qquad (Eq.\ 2)$$

$$CH_4 + 1/2O_2 \rightarrow CO + 2H_2 \qquad \Delta H_{298K} = -36\ kJ\ mol^{-1} \qquad (Eq.\ 3)$$

In contrast to SRM and DRM methods, POM is a mildly exothermic reaction. For this reason, POM is seen as an energy-saving process, and is considered the most economic technology for syngas production [7,8]. Moreover, the molar ratio of H_2/CO in the POM reaction is close to 2, which is suitable for the production of methanol and higher hydrocarbons through the Fischer-Tropsch process [9,10]. Besides, POM can handle a large volume of the feed gas with only a small amount of catalyst [11,12].

Usually, the POM process into syngas occurs in two steps [4,13]. In the first step, CH_4 is combusted by O_2 to produce CO_2 and H_2O (Eq. (4)), and then the remaining unreacted CH_4 is reformed with water (Eq. (5)) and CO_2 (Eq. (6)) to produce CO and H_2 [13,14]. These reactions are always accompanied by the water gas-shift equilibrium (Eq. (7)) [13].

$$CH_4 + 2O_2 \rightleftarrows CO_2 + 2H_2O \qquad \Delta H_{298} = -803\ kJ\ mol^{-1} \qquad (Eq.\ 4)$$

$$CH_4 + H_2O \rightleftarrows CO + 3H_2 \qquad \Delta H_{298} = +206\ kJ\ mol^{-1} \qquad (Eq.\ 5)$$

$$CH_4 + CO_2 \rightleftarrows 2CO + 2H_2 \qquad \Delta H_{298} = +247\ kJ\ mol^{-1} \qquad (Eq.\ 6)$$

$$CO_2 + H_2 \rightleftarrows CO + H_2O \qquad \Delta H_{298} = -41\ kJ\ mol^{-1} \qquad (Eq.\ 7)$$

After nearly 100 years of investigation on the catalytic partial oxidation of methane into syngas, numerous catalyst formulations have been tested. They can be divided basically into three main types: (1) nickel, cobalt, or iron catalysts, (2) transition metal carbide catalysts, and (3) noble metal catalysts [15,16]. Currently, the industrial catalysts used for POM are primarily nickel and noble metal supported catalysts [1]. Nickel-based catalysts have been widely investigated due to their low cost; however, they are easily deactivated owing to carbon deposition and metal loss at temperatures higher than 700 °C [4,5,17]. To improve thermal stability and activity and decrease carbon deposition, other components like noble metals (Pd, Pt, Rh, Ru, etc.) are added to Ni catalysts. These noble metals are more active, less sensitive to coke formation and have higher capacity to oxidize hydrocarbons, but are expensive. Therefore, bimetallic catalysts with Ni and noble metals have been proposed to promote methane conversion [15,17]. Palladium is one of the most effective noble metals used for methane conversion processes [18–20]. The support plays also an important role on the POM process [21,22]. Most catalysts show high activity when metals are dispersed on a reducible oxide support [4]. Cerium oxide (CeO_2) is one of the most significant reducible oxide supports used in industrial catalysis as it reduces carbon deposition and has a remarkable oxygen storage/exchange capacity due to facile oxygen vacancy formation and change of oxidation states between Ce^{3+} and Ce^{4+} [19,23].

The main objective of the present investigation is to develop an effective bimetallic Ni–Pd/CeO_2 catalytic system for POM to produce syngas at low temperature. To that end, a series of monometallic Ni, Pd, and Pd–Ni bimetallic catalysts supported on CeO_2 were prepared, characterized and tested. Two different methods were used to prepare the catalysts, dry ball milling (BM) and conventional incipient wetness impregnation (IWI). The BM technique is a green technology with enormous potential for the preparation of catalysts; it has an easy operation and it is fast, cost-effective and environmentally friendly [24–26].

Materials and methods

Preparation of CeO_2

Cerium nitrate hexahydrate ($Ce(NO_3)_3{\cdot}6H_2O$, 99.5%) and palladium (II) nitrate ($Pd(NO_3)_2$, 93%) were purchased from Alfa Aesar. Nickel (II) nitrate hexahydrate ($Ni(NO_3)_2{\cdot}6H_2O$, 98%) was obtained from Fisher chemical. Ammonia solution (NH_3, 28%) was obtained from Scharlab. All reagents were used without further purification. Cerium dioxide (CeO_2) was obtained by adding dropwise NH_3 to an aqueous solution of $Ce(NO_3)_3{\cdot}6H_2O$ until the pH reached a value between 9 and 10 and a yellowish precipitate was obtained. After that, the precipitated was filtered and washed thoroughly with deionized water. The precipitate was dried overnight at 90 °C and calcined at 650 °C for 4 h (5 °C min^{-1}).

Preparation of catalysts by mechanochemical method

Monometallic Pd(x)/CeO_2/BM (x = 0.5, and 1 wt%) and Ni(y)/CeO_2/BM (y = 0.5 wt%) catalysts were prepared via ball mill (labeled as BM). $Ni(NO_3)_2{\cdot}6H_2O$ and $Pd(NO_3)_2$ were used as Ni and Pd precursors, respectively. The desired amounts of metal nitrates were mixed directly with CeO_2 in a zirconium oxide vessel using a Fritsch Pulverisette 23 mini-mill apparatus and one zirconium oxide ball of 15 mm diameter (ball to powder ratio, BPR = 10.2). Two different routes were used to prepare the bimetallic Pd(x)-Ni(y)/CeO_2/BM catalysts (x = 0.06–1 wt%, y = 0.5 to 1.44 wt%; x + y = 1.5) by the BM method: (1) co-BM and (2) sequential-BM. In the co-BM method, the bimetallic Pd–Ni/CeO_2/BM catalysts were prepared in one-step by milling together CeO_2 and the metal precursors. In the sequential-BM method, firstly, one of the metal precursors was mixed with cerium oxide by BM, and in the next step the other precursor was added and subjected again to BM. These samples were labeled as Pd–CeO_2/BM/Ni/BM or Ni–CeO_2/BM/Pd/BM

depending if ceria was first milled with the Pd precursor or with the Ni precursor, respectively. The effect of ball mill frequency (15, 30 and 50 Hz) and milling time (5–40 min) was also investigated. All the fresh catalysts were used without any further treatment.

Preparation of catalysts by incipient wetness impregnation

Monometallic Pd, Ni, and bimetallic Pd–Ni catalysts were also prepared by conventional incipient wetness impregnation for comparison (labeled as IWI). For the preparation of monometallic Ni(y)/CeO_2/IWI (y = 0.5 wt%) and Pd(x)/CeO_2/IWI (x = 0.5, and 1 wt%), $Ni(NO_3)_2{\cdot}6H_2O$ and $Pd(NO_3)_2$ aqueous solutions were used as precursors. Samples were dried at 90 °C and calcined at 650 °C for 4 h (5 °C min^{-1}). Two different routes were used to prepare the bimetallic Pd(x)-Ni(y)/CeO_2/IWI catalysts (x = 0.06–1 wt%, y = 0.5 to 1.44 wt%; x + y = 1.5) by the IWI method: (1) co-IWI and (2) sequential-IWI. In the co-IWI method, the Pd–Ni/CeO_2/IWI catalysts were prepared in one-step, while in sequential-IWI two subsequent impregnations were carried out, with a calcination step at 650 °C for 2 h between each impregnation. These samples were labeled as Ni–CeO_2/IWI/Pd/IWI or Pd–CeO_2/IWI/Ni/IWI depending if the first impregnation was carried out with the Ni or the Pd precursor, respectively. No further treatments were performed on the calcined samples before the catalytic test.

Catalytic tests

The catalytic performance of the catalysts for the POM process was evaluated in a continuous-flow fixed-bed quartz tubular reactor. Reactions were carried out at atmospheric pressure between 300 and 550 °C using a mixture of CH_4:air:N_2 = 4:11:85 (molar, CH_4/O_2 = 1.73) and F/W = 60 L h^{-1} g^{-1} (gas hourly space velocity GHSV = 12 × 10^3 h^{-1}). Typically, 0.1 g of catalyst was mixed with silicon carbide to obtain a fixed bed volume of 0.5 cm^3. The reactor was heated in an electrical furnace (Carbolite CTF) and the temperature in the center of the catalyst bed was measured with a type K thermocouple; no axial thermal gradients were measured. CH_4 conversion (X_{CH4}) and syngas selectivities (S_{H2}, S_{CO}) were evaluated from 300 °C to 550 °C in steps of 50 °C. At each temperature, a dwell time of 45 min was applied, thus ensuring steady-state conditions. The reaction products were analyzed online every 4 min with a gas chromatograph (Varian CP-4900) equipped with Molecular Sieve of 5 Å, Plot U and Stabilwax columns for a complete analysis of products. The methane conversion (X_{CH4}) (Eq. (8)), selectivity of hydrogen (S_{H2}) (Eq. (9)), selectivity of carbon monoxide (S_{CO}) (Eq. (10)), and yield of syngas (Y_{sg}) (Eq. (11)) were calculated according to the following equations:

$$x_{CH4}(\%) = \frac{F_{inCH_4} - F_{outCH_4}}{F_{inCH_4}} \times 100 \quad \text{(Eq. 8)}$$

where F_{inCH_4} and F_{outCH_4} are the inlet and outlet molar flow of methane, respectively

$$S_{H2}(\%) = \frac{moles\ of\ H_2\ produced}{moles\ of\ (H_2 + CO + CO_2) produced} \times 100 \quad \text{(Eq. 9)}$$

$$S_{CO}(\%) = \frac{moles\ of\ CO\ produced}{moles\ of\ (H_2 + CO + CO_2) produced} \times 100 \quad \text{(Eq. 10)}$$

$$Y_{sg}(\%) = \frac{x_{CH_4} \times (S_{H2} + S_{CO})}{100} \quad \text{(Eq. 11)}$$

Catalyst characterization

Characterization of the surface was accomplished by X-ray photoelectron spectroscopy (XPS) with a SPECS system equipped with a XR50 source operating at 250 W and a Phoibos 150 MCD-9 detector. The pass energy of the high-resolution spectra was set at 0.1 eV. Binding energy (BE) values were referred to the Ce^{4+} $3d_{5/2}$ peak at 916.9 eV. The microstructure of the catalysts was investigated with high resolution transmission electron microscopy (HRTEM) and energy-dispersive X-ray analysis (EDX) using a FEI TECNAI F20 instrument operated at 200 kV. Raman spectroscopy was performed using a Renishaw inViaQontor confocal Raman microscope equipped with a 532.1 ± 0.3 nm laser with a nominal 100 mW output power directed through a specially adapted Leica DM2700 M microscope (x50 magnification). Spectra were acquired in two ranges, 50-800 cm^{-1} and 1000-2000 cm^{-1}, with an exposure time of 0.5 s, 1% of maximum laser power and 18 repetitions. Temperature programmed reduction (TPR-H_2) was performed with a Chemstar apparatus with TCD detector. Samples were first treated at 450 °C in Ar (50 mL min^{-1}, 10 °C min^{-1}), and then TPR was carried out from 30 to 850 °C (10 °C min^{-1}) under 10% H_2 and kept at this temperature for 30 min.

Results and discussion

Characterization of fresh catalysts

Raman spectroscopy

The Raman spectra recorded for the bimetallic Pd–Ni/CeO_2 catalysts prepared by BM and IWI methods before the catalytic tests are shown in Fig. 1. In all cases, the Raman were dominated by the symmetrical stretching mode of the CeO_2 lattice structure (F_{2g} mode) at ~464 cm^{-1} [27]. Additionally, for the bimetallic Pd–Ni/CeO_2 catalyst prepared by BM, Raman spectra indicated a weak band at ~1050 cm^{-1}, which corresponds to the symmetric ν_1 stretching mode of the nitrate anion [28,29]. The NO_3^- band was absent in the bimetallic catalysts prepared by IWI because nitrate residues disappeared following the calcination treatment performed at 650 °C. Also, for the bimetallic Pd–Ni/CeO_2 catalyst prepared by IWI, a broad band from ~530 to 620 cm^{-1} is observed, which can be ascribed to NiO species [29], although a defect-induced vibrational mode of ceria lattice defects in the ceria structure, such as oxygen vacancies, cannot be discarded (~595 cm^{-1}, D band) [30].

Transmission electron microscopy (HRTEM)

With the aim of understanding the microstructure of the catalysts, the Pd–Ni dispersion and the possible interactions between metal and support, high resolution transmission

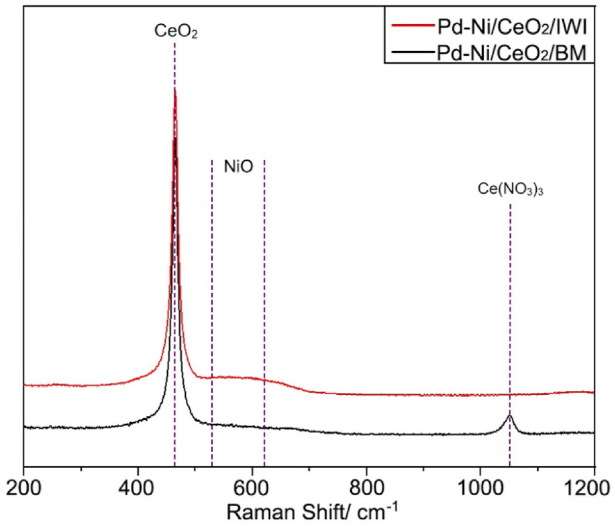

Fig. 1 – Raman spectra of bimetallic catalysts with 1 wt% Pd and 0.5 wt% Ni supported on CeO_2 prepared by BM at 50 Hz for 20 min (black), and IWI (red). (For interpretation of the references to color/colour in this figure legend, the reader is referred to the Web version of this article.)

electron microscopy (HRTEM) and energy-dispersive X-ray analysis (EDX) were used (Fig. 2). A representative image of the monometallic Pd/CeO_2 catalyst prepared by BM is shown in Fig. 2a. The sample is very homogeneous and contains sub-nanometric Pd entities (some of them indicated with arrows in the image), which are well dispersed over the CeO_2 support. A larger Pd particle is highlighted with a dashed square. The Fourier Transform (FT) image of this area is shown in the inset and shows spots at 1.9 Å from CeO_2 (220) planes and at 2.2 Å from Pd (111) planes. The EDX spectrum recorded in the same area confirms the nature of the particle and shows the simultaneous occurrence of Ce, Pd and O (the Cu signal originates from the TEM grid). Fig. 2b corresponds to the bimetallic Pd–Ni/CeO_2 catalysts prepared by IWI method. It is difficult to distinguish any Pd, Ni or Pd–Ni particle in TEM analysis, which indicates an excellent dispersion of Ni and Pd on the CeO_2 support. The EDX spectrum recorded from the area enclosed by the square shows only weak Pd signals; no signals of Ni are observed, probably due to the low loading of Ni (0.5 wt %). Fig. 2c shows the microstructure of the bimetallic Pd–Ni/CeO_2 catalysts prepared by the BM method. The mechano-chemical preparation of Pd–Ni/CeO_2 creates an amorphous layer around the ceria crystallites (marked between arrows). This shell exhibits an average thickness of about 2–4 nm. The EDX spectrum recorded from the area enclosed by the square conclusively identified both Pd and Ni in this amorphous shell. The amorphous shell is similar to that recently reported in Pd/CeO_2 catalysts prepared by BM [31] and corresponds to an unprecedented architecture.

X-ray photoelectron spectroscopy (XPS)

The surface composition of the bimetallic Pd–Ni/CeO_2 catalysts prepared by ball milling was analyzed by X-ray

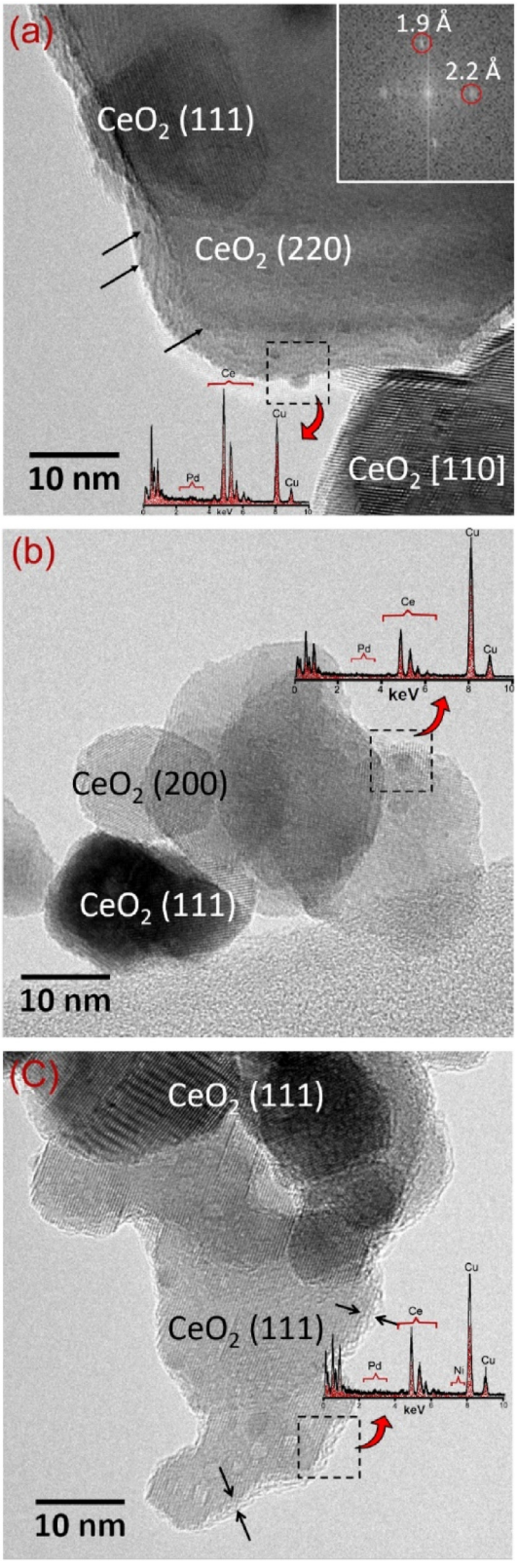

Fig. 2 – HRTEM images of (a) monometallic Pd (1)/CeO_2 catalyst prepared by BM at 50 Hz for 20 min; (b) bimetallic Pd (1)-Ni(0.5)/CeO_2 catalyst prepared by IWI; (c) bimetallic Pd (1)-Ni(0.5)/CeO_2 catalyst prepared by BM at 50 Hz for 20 min.

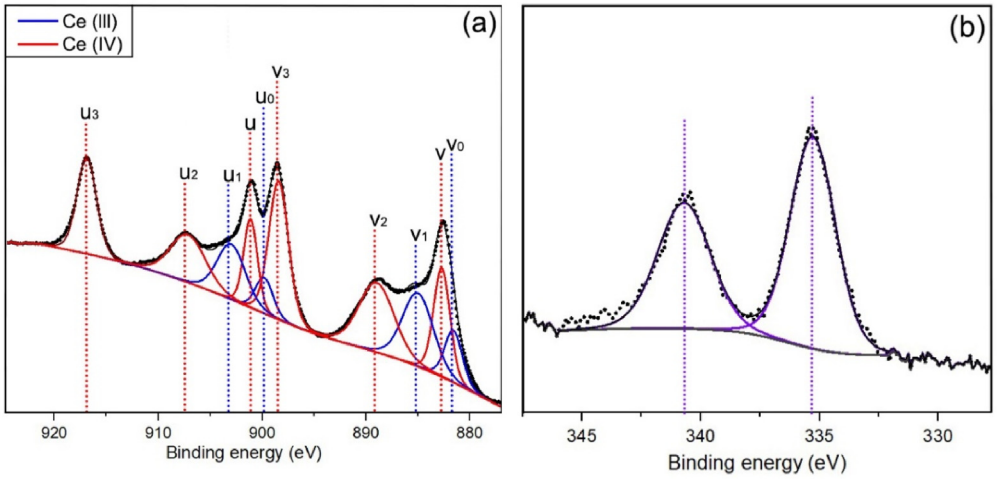

Fig. 3 – Ce 3d (a) and Pd 3d (b) X-ray photoelectron spectra of the bimetallic Pd (1)-Ni(0.5)/CeO_2/BM catalyst (50 Hz for 20 min).

photoelectron spectroscopy (XPS). Fig. 3a shows the Ce 3d spectrum. The peaks marked as v (882.7 eV), v_2 (889 eV), v_3 (899.8 eV), u (901.1 eV), u_2 (907.1eV) and u_3 (916.9 eV) correspond to the presence of Ce^{4+} species, and those labeled as v_0 (881.6 eV), v_1 (885 eV), u_0 (898.4 eV), and u_1 (903 eV) correspond to Ce^{3+} species [32,33]. About 40% of cerium at the surface appears as Ce^{3+} species. Fig. 3b shows the Pd 3d spectrum. A single doublet corresponding to the $3d_{5/2}$ and $3d_{3/2}$ splitting is present, with a binding energy for $3d_{5/2}$ at 335.3 eV, which corresponds well to reduced Pd. The surface Pd/Ce and Ni/Ce atomic ratios are 0.09 and 0.04, respectively, which points to an excellent dispersion of the two metals over the ceria support.

Temperature programmed reduction (H_2-TPR)

The H_2-TPR profiles recorded for the investigated samples are shown in Fig. 4. All the samples show a high-temperature reduction peak located above 700 °C, which corresponds to the bulk reduction of CeO_2, as reported elsewhere [34]. However, it is worth mentioning that the high-temperature peak is shifted to lower temperatures when samples are prepared by the BM method with respect to analogous samples prepared by IWI. The Ni/CeO_2/IWI catalyst shows a broad H_2 consumption at ~450 °C, which corresponds to the reduction of NiO strongly interacting with the CeO_2 support [35,36], according to an enhanced metal-support interaction following calcination [37,38]. In contrast, the H_2 consumption on the Ni/CeO_2 catalyst prepared by BM appears at much lower temperature (~185 °C) and with higher intensity, which can be assigned to the reduction of well-dispersed NiO species [39]. It is interesting to note that the ball mill method notably improves the metal reducibility at lower temperature. The monometallic catalyst Pd/CeO_2 prepared by BM method a broad reduction peak centered at ~285 °C, which can be assigned to the reduction of PdO species anchored on CeO_2 [40,41].

The bimetallic Pd–Ni/CeO_2 catalysts prepared by both IWI and BM methods show similar H_2-TPR profiles with a broad H_2 consumption at about ~250 °C, due to PdO–NiO reduction.

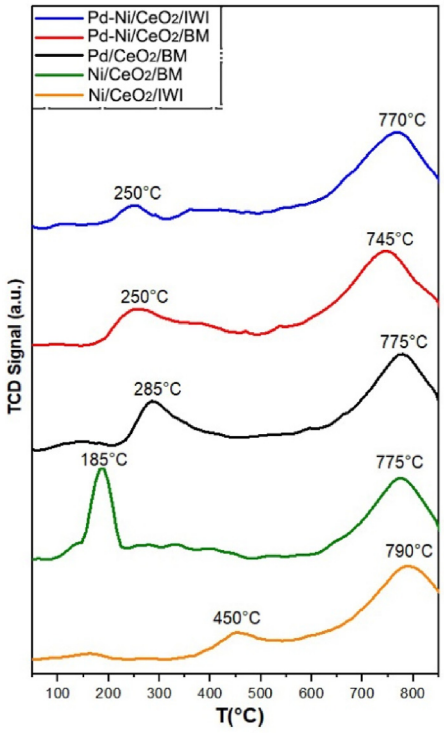

Fig. 4 – H_2-TPR profiles corresponding to Pd (1)/CeO_2/BM (black), Ni(0.5)/CeO_2/BM (green), Ni(0.5)/CeO_2/IWI (orange), Pd (1)-Ni(0.5)/CeO_2/IWI (blue) and Pd (1)-Ni(0.5)/CeO_2/BM (red). Ball mill conditions were 50 Hz for 20 min. (For interpretation of the references to color/colour in this figure legend, the reader is referred to the Web version of this article.)

Compared to Pd/CeO_2 monometallic catalysts, in the bimetallic Pd–Ni/CeO_2 catalysts the reduction appears at a lower temperature, indicating that the addition of Ni facilitates the reduction of PdO. In other words, there is a strong synergy between both metals, which is in accordance to the HRTEM results (Fig. 2c).

Catalytic tests

The temperature-dependent catalytic performance of the different catalysts prepared followed similar patterns. As a representative example, Fig. 5 shows the molar flow rates of reactants (methane and oxygen) and products (syngas, water and carbon dioxide) from 300 to 550 °C of bimetallic Pd–Ni/CeO_2 catalysts prepared by BM (Fig. 5a) and IWI (Fig. 5b) methods. According to thermodynamics, the conversion of methane increases progressively with temperature. However, significant differences are observed between BM and IWI catalysts. For the bimetallic catalyst prepared by BM, all the oxygen is consumed at 450 °C and from this temperature the consumption of methane runs parallel to the consumption of water and the production of syngas is observed. Therefore, this performance below 450 °C obeys to the equation: $CH_4 + 2O_2 \rightarrow CO_2 + 2H_2O$. At higher temperatures, when all the oxygen is consumed, the reaction that takes place is the methane steam reforming reaction: $CH_4 + H_2O \rightleftarrows CO + 3H_2$, where the conversion of methane is accompanied by the consumption of H_2O and the production of syngas increases drastically. Simultaneously, the dry reforming of methane likely occurs: $CH_4 + CO_2 \rightleftarrows 2CO + 2H_2$. This mechanisms corresponds to the well-known "combustion and reforming reaction (CRR)" mechanism outlined in the introduction section [16,42], although a detailed kinetic analysis out of thermodynamic control would be necessary to discuss the reaction mechanism in more detail [43,44]. Similar trend distribution and appearance of products are obtained when the bimetallic catalyst was prepared by the conventional IWI method, confirming that a similar reaction mechanism takes place independently of the preparation method. However, all the reactions occur at higher temperatures, indicating lower catalytic activity.

Considering the two consecutive steps involved in the POM reaction and given that below 450 °C the production of syngas is not significant, only the performance of the catalysts at temperatures above 450 °C will be considered further. Table 1 compiles the catalytic results of all prepared samples in terms of methane conversion (x_{CH4}), H_2 selectivity (S_{H2}), CO selectivity (S_{CO}) and yield of syngas (Y_{sg}). Bare CeO_2 results are also included as a blank test, as well as chemical equilibrium values.

The CeO_2 support in the absence of Pd and Ni is totally inactive for POM under the reaction conditions tested. Moreover, the catalytic activity results for the catalysts with 0.5 wt % Ni supported on CeO_2 prepared by either IWI or BM methods showed low methane conversion and the formation of syngas was not observed at all. On the other hand, it is clear that the catalytic activity of Pd/CeO_2 is much greater than Ni/CeO_2, as the methane conversion values for Pd/CeO_2 catalysts at 550 °C doubled those obtained over Ni/CeO_2 catalysts and the syngas yield was 42–48%. The milling parameters had negligible effect on the catalytic performance of the monometallic catalysts, as methane conversion at 550 °C oscillated between 51 and 55% and syngas yield from 42 to 47%.

From Table 1, it can be clearly seen that the cooperative effect between Pd and Ni in the bimetallic catalysts is remarkable, with a dramatic increase in both the methane conversion and the syngas yield compared to monometallic catalysts. At 550 °C, bimetallic Pd–Ni/CeO_2 catalysts show methane conversion levels from 62 to 75%, selectivity towards H_2 of 64–66%, selectivity towards CO of 19–24%, and syngas yield between 52 and 67%. These results demonstrate that the synergy between Pd and Ni supported on CeO_2 yields catalysts with improved activity and selectivity in the POM with respect to monometallic Ni/CeO_2 and Pd/CeO_2.

The preparation method (BM vs. IWI), the order of incorporation of the metals (co-BM/co-impregnation vs. sequential BM/IWI) play an important role on the catalytic performance of the bimetallic Pd–Ni/CeO_2 catalysts. Fig. 6a shows the methane conversion at different temperatures for the bimetallic Pd (1)-Ni(0.5)/CeO_2 catalysts prepared by co-impregnation and sequential-impregnation. Interestingly, at low temperature (450 °C) the methane conversion of the catalysts prepared by sequential impregnation is much higher than that of the catalyst prepared by co-impregnation, regardless of the order of addition used for Pd and Ni. In contrast, at high temperatures (500 and 550 °C), the methane conversion attained by the catalyst prepared by co-impregnation is higher than those of the catalysts prepared

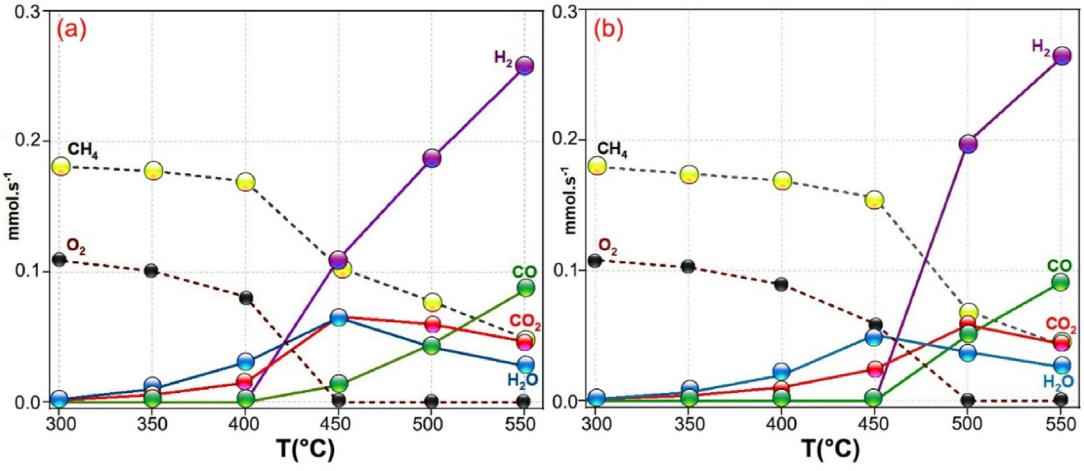

Fig. 5 – Molar flowrates recorded for bimetallic catalysts Pd (1)-Ni(0.5)/CeO_2 prepared by BM at 50 Hz for 20 min (a) and IWI (b) methods. GHSV = 12 × 10^3 h^{-1}, F/W = 60 L h^{-1} g^{-1}.

Table 1 – Methane conversion, hydrogen and carbon monoxide selectivity values and syngas yields obtained over bare CeO_2, Ni/CeO_2, Pd/CeO_2 and Pd–Ni/CeO_2 bimetallic catalysts prepared by incipient wetness impregnation (IWI) and dry ball milling (BM) using different synthesis parameters and metal loading values. Reaction conditions: CH_4:air:N_2 = 4:11:85, F/W = 60 L h^{-1} g^{-1}, GHSV = 12 × 10^3 h^{-1}.

Sample	Hz	min	wt.%Pd	wt.%Ni	$x_{CH_4}^{450°C}$	$x_{CH_4}^{550°C}$	$S_{H_2}^{550°C}$	$S_{CO}^{550°C}$	$Y_{syngas}^{550°C}$
Equilibrium	-	-	-	-	51.3	77.9	67.2	26.3	70.9
CeO_2/BM	50	10	0	0	0	0	0	0	0
Ni/CeO_2/BM	50	10	0	0.5	3.2	22	0	0	0
Ni/CeO_2/IWI	-	-	0	0.5	3	18.6	0	0	0
Pd/CeO_2/BM	50	10	0.5	0	32.6	52.7	63.3	17.7	42.7
Pd/CeO_2/IWI	-	-	0.5	0	39.7	51	63.8	23	44.5
Pd/CeO_2/BM	50	10	1	0	30.5	53.2	64.8	19.3	44.8
Pd/CeO_2/IWI	-	-	1	0	34.5	57.4	64.5	19.4	48.2
Pd/CeO_2/BM	50	20	1	0	32.7	55.6	65.2	20.2	47.6
Pd/CeO_2/BM	15	10	1	0	35.2	54.9	63.5	18	44.7
Pd/CeO_2/BM	30	10	1	0	31.4	51	64	18.2	41.9
Pd–Ni/CeO_2/BM	15	10	1	0.5	36.4	62.4	64.2	19.2	52.1
Pd–Ni/CeO_2/BM	30	10	1	0.5	39.9	67.1	64.9	20.5	57.4
Pd–Ni/CeO_2/BM	50	10	1	0.5	44	71.8	65.5	21.7	62.7
Pd–CeO_2/BM/Ni/BM	50	10	1	0.5	42.5	71.6	65.5	22	62.6
Ni–CeO_2/BM/Pd/BM	50	10	1	0.5	41.6	68	64.9	20.5	58.1
Pd–Ni/CeO_2/BM	50	5	1	0.5	37.5	67.2	65.5	20.7	57.9
Pd–Ni/CeO_2/BM	50	15	1	0.5	38	66.3	65.5	21.2	57.5
Pd–Ni/CeO_2/BM	50	20	1	0.5	42.1	72.4	66	22	63.7
Pd–Ni/CeO_2/BM	50	40	1	0.5	41.4	71.5	65.8	21.7	62.6
Pd–Ni/CeO_2/BM	50	20	0.75	0.75	37.9	67.4	65.4	21.7	58.7
Pd–Ni/CeO_2/BM	50	20	0.5	1	35.5	68.2	65.3	21.7	59.4
Pd–Ni/CeO_2/BM	50	20	0.25	1.25	37.7	70.6	65.9	23.8	63.4
Pd–Ni/CeO_2/BM	50	20	0.12	1.38	40.8	69.5	65.9	23.6	62.2
Pd–Ni/CeO_2/BM	50	20	0.06	1.44	36.6	69.5	66	23.1	62
Ni–CeO_2/IWI/Pd/IWI	-	-	1	0.5	38.5	51.5	64.6	19.5	54
Pd–CeO_2/IWI/Ni/IWI	-	-	1	0.5	42.2	71.7	66	21.8	63
Pd–Ni/CeO_2/IWI	-	-	1	0.5	12.6	75.8	66.1	22.8	67.4
Pd–Ni/CeO_2/IWI	-	-	0.75	0.75	11.6	74.8	66.2	22.5	66.3
Pd–Ni/CeO_2/IWI	-	-	0.5	1	7.7	74.4	66.3	22.8	66.3
Pd–Ni/CeO_2/IWI	-	-	0.25	1.25	6.9	70	66	21.8	63
Pd–Ni/CeO_2/IWI	-	-	0.12	1.38	2.8	67.7	65.8	23	60.2
Pd–Ni/CeO_2/IWI	-	-	0.06	1.44	3.3	65.4	66	22.9	62.6

by sequential impregnation. No remarkable differences were observed between bimetallic catalysts prepared by co-BM or sequential-BM (Fig. 6b). In all cases, the methane conversion was similar at each temperature. In any case, the addition of Pd first gives better catalytic results than when Ni is first incorporated, which points to a better catalytic performance when Pd interacts strongly with CeO_2, as opposed to Ni.

On the other hand, the effect of milling conditions (frequency and time) on the catalytic activity of bimetallic Pd–Ni/CeO_2/BM catalyst at different temperatures is shown in Fig. 6c and d. The energy applied during the ball milling in terms of frequency of vibration has a strong effect on catalytic activity; the higher the energy the better the catalytic activity of the catalyst (Fig. 6c). Therefore, it is clear that high-energy milling has a beneficial influence on the number and quality of the active sites [45,46]. This work adds an additional evidence that ball milling is able to create unprecedented architectures that can exhibit outstanding catalytic activity. The ball milling time is another important factor that can affect catalytic performance. Fig. 6d shows the effect of the milling time (from 5 to 40 min) on the methane conversion values. A good compromise between methane conversion and milling time is found for the catalyst prepared using 20 min of milling time. Accordingly, a ball milling frequency of 50 Hz for 20 min appears as the optimal synthesis conditions.

An important aspect regarding bimetallic catalysts is the relative amount of the two metals involved. In our case, it should be also considered that the cost of Pd is much higher than that of Ni, which obviously has a direct impact on the final cost of the catalyst. Fig. 7 shows the methane conversion and syngas yield at 450 °C and 550 °C exhibited by Pd–Ni/CeO_2/BM and Pd–Ni/CeO_2/IWI catalysts containing different amounts of Pd and Ni but keeping the total metal loading at 1.5 wt% (Pd wt.% from 0.06 to 1% and Ni wt.% from 0.5 to 1.44%). Two aspects merit particular attention. First, it is very interesting to observe that at 450 °C both the methane conversion and syngas yield are much higher for all the catalysts prepared by BM with respect to their respective counterparts prepared by the IWI method. This clearly demonstrates that very reactive and specific active sites are created by the BM method, which are highly active for the POM process at low temperature. At 550 °C, the catalytic performance of Pd–Ni/CeO_2/BM and Pd–Ni/CeO_2/IWI catalysts are similar. Second, the effect of the Pd amount on the catalytic performance is lower than expected and depends also on the preparation method. For the Pd–Ni/CeO_2/IWI catalysts, a trend is observed

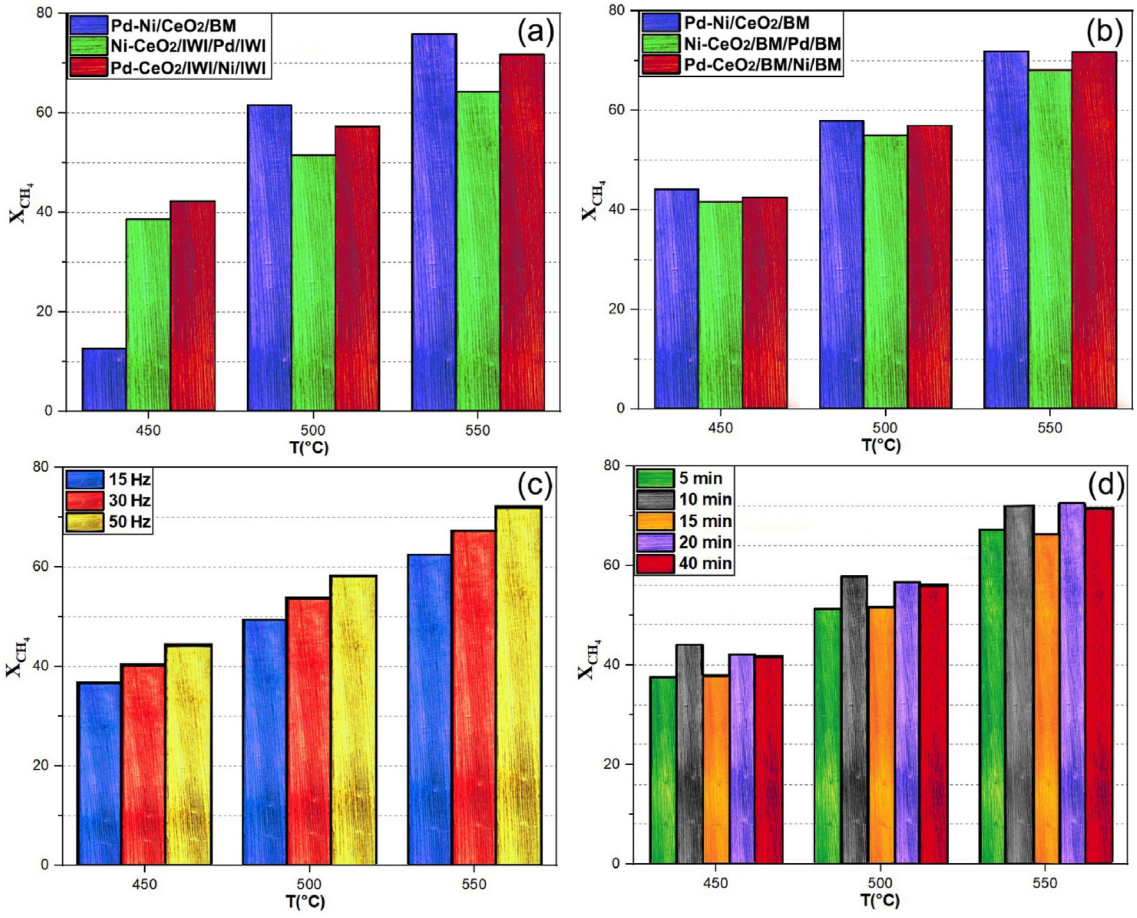

Fig. 6 – Conversion of methane at 450, 500 and 550 °C over Pd–Ni/CeO_2 catalysts prepared by IWI (a), Pd–Ni/CeO_2 catalysts prepared by BM at 50 Hz for 10 min (b), Pd–Ni/CeO_2/BM prepared at different milling frequency for 10 min (c), and Pd–Ni/CeO_2/BM prepared at 50 Hz for different milling time (d). GHSV = 12 × 10^3 h^{-1}, F/W = 60 L h^{-1} g^{-1}.

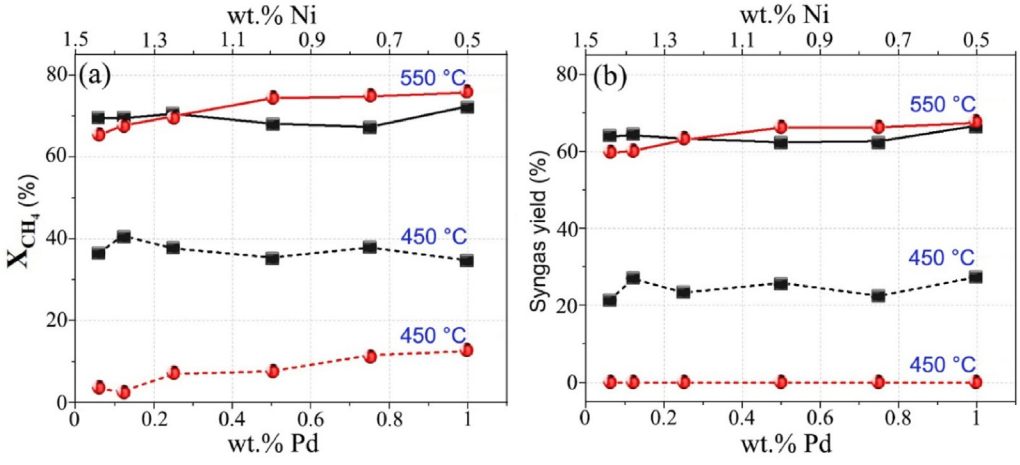

Fig. 7 – Conversion of methane (a) and yield of syngas (b) for the bimetallic Pd(x)-Ni(y)/CeO_2 catalysts containing different amounts of Pd and Ni prepared by BM (black) and IWI (red) methods at 450 °C and 550 °C. All catalysts contain a total metal loading of 1.5 wt%. GHSV = 12 × 10^3 h^{-1}, F/W = 60 L h^{-1} g^{-1}. (For interpretation of the references to color/colour in this figure legend, the reader is referred to the Web version of this article.)

between methane conversion and Pd content: the higher the Pd amount the higher the conversion of methane. This is not the case of the Pd–Ni/CeO_2/BM catalysts, where both the methane conversion and syngas yield are rather unsensitive of the relative amounts of Pd and Ni in the range studied. It should be highlighted that the Ni/CeO_2/BM sample showed

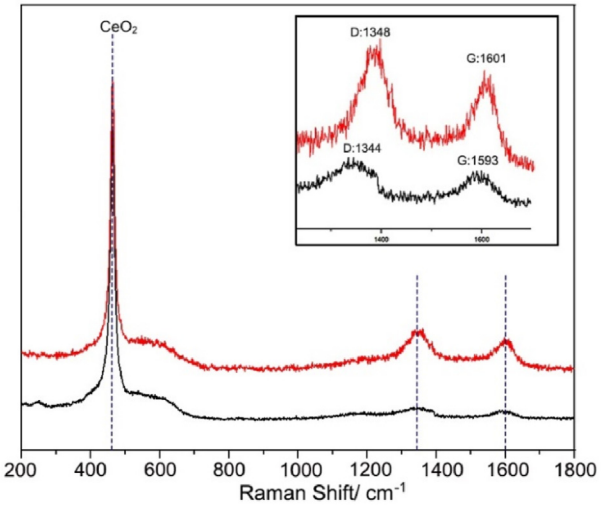

Fig. 8 – Raman spectra of bimetallic Pd (1)-Ni(0.5)/CeO_2 catalysts prepared by BM at 50 Hz for 20 min (black), and IWI (red) after reaction (CH_4:air:N_2 = 4:11:85, F/W = 60 L h^{-1} g^{-1}, GHSV = 12 × 10^3 h^{-1}). (For interpretation of the references to color/colour in this figure legend, the reader is referred to the Web version of this article.)

low methane conversion (3.2% at 450 °C and 22% at 550 °C, Table 1) and no syngas production, whereas with only 0.06 wt % Pd the methane conversion increased up to 36.6 and 69.5% at 450 and 550 °C, respectively, and syngas yield was 62%. Certainly, the bimetallic Pd–Ni system appears as a particularly appealing metal combination for POM. It has recently been shown by using DFT calculations that the substitution of Ce by Pd ions in the surface of the catalysts originates highly active and stable species based on $Pd_xCe_{1-x}O_\delta$ which are highly effective in the rapid C–H bond activation [47,48]. From the HRTEM images, we cannot conclude if Pd substitutes Ce in the ceria structure but, in any case, we have evidence that both Pd and Ni are highly dispersed at the subnanometric level. At low temperature (450 °C), where the bimetallic Pd–Ni catalysts prepared by BM exhibit a particular high activity for POM as outlined above, the best performance (both methane conversion and syngas yield) was observed for Pd–Ni/CeO_2/BM with 0.12 wt% Pd and 1.38 wt% Ni.

Characterization of the catalysts after reaction

The Raman spectra recorded on the samples Pd–Ni/CeO_2/BM, and Pd–Ni/CeO_2/IWI after the catalytic test discussed above are shown in Fig. 8. In all cases, the position of the F_{2g} band of CeO_2 did not shift after the catalytic test with respect to the values recorded before reaction (Fig. 1), and the residual nitrate signals in the sample Pd–Ni/CeO_2/BM disappeared after reaction due to decomposition. In addition, the two characteristic graphite D and G bands at about ~1345 and ~1595 cm^{-1} [49,50] were observed in the Raman spectra of the catalysts after reaction, being their relative contribution in the spectra considerably more intense in the case of the bimetallic sample prepared by impregnation. Therefore, less coke deposition occurred on the bimetallic sample prepared by ball milling. Catalyst Pd–Ni/CeO_2/BM was studied by HRTEM and EDX (Fig. 9). Interestingly, a large number of voids are identified in the ceria crystallites, which were not visible in the sample before reaction (Fig. 2c). These are tentatively ascribed to clusters of oxygen vacancies, probably in contact with the metals, created under the reducing environment created by syngas during POM. On the other hand, even if the amorphous shell is no longer observed after the catalytic test, Pd and or Ni particles escape detection in HRTEM but are present in EDX analyses, indicating that the high dispersion of the metals is maintained during the catalytic reaction. Also, and in accordance with the Raman results, coke is identified by its characteristic spacing at 3.8 Å, which corresponds to the (0001) interplanar spacing of poorly ordered graphite. However, the amount of deposited coke is rather low.

Stability tests

In order to prove the long-term performance of the catalysts, stability tests for more than 100 h at 550 °C were carried out. Since bimetallic catalysts showed good methane conversion and selectivity to syngas (Table 1), Pd–Ni/CeO_2 catalysts with 1 wt% Pd and 0.5 Ni loading prepared by both IWI and BM

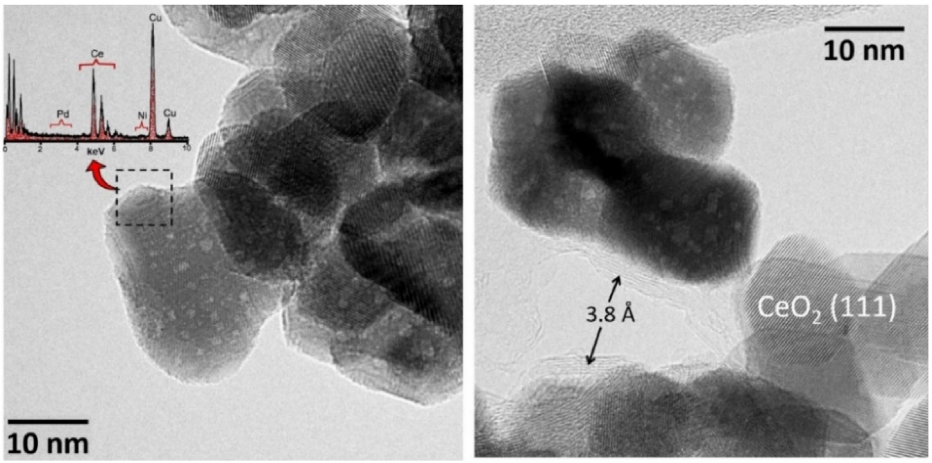

Fig. 9 – HRTEM images of the bimetallic Pd (1)-Ni(0.5)/CeO_2/BM catalyst (50 Hz for 20 min) after the catalytic test.

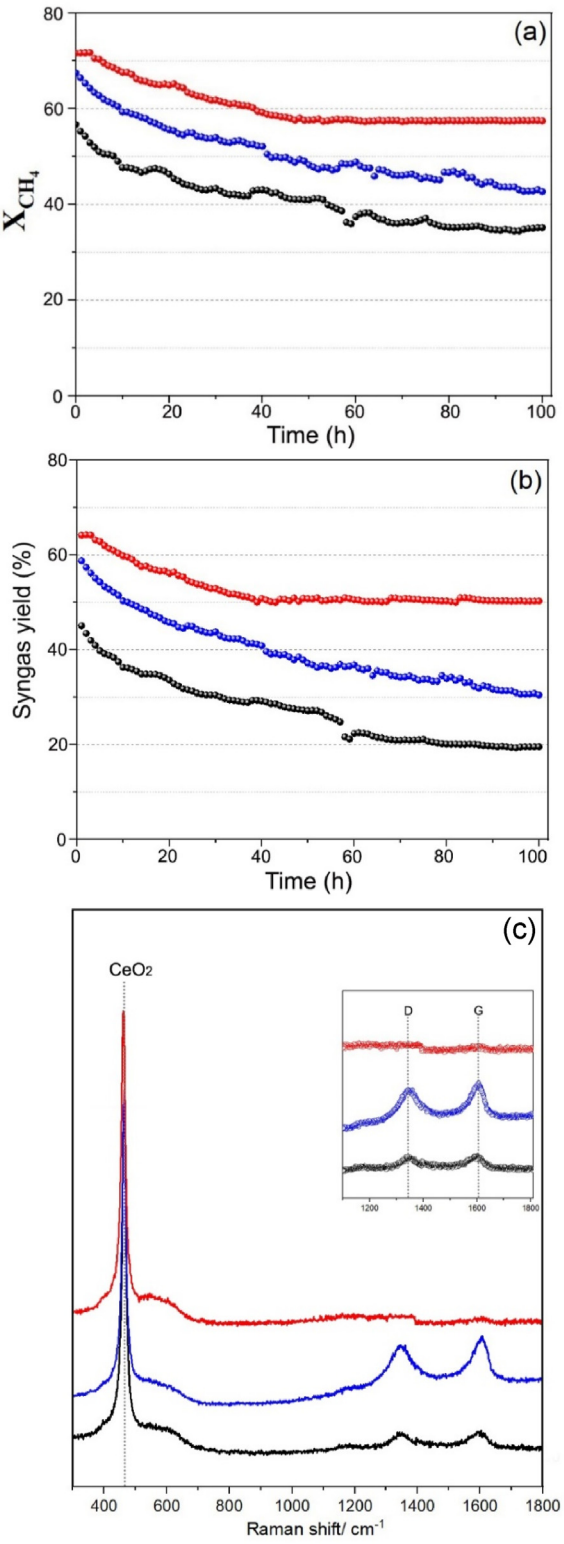

Fig. 10 – Methane conversion (a) and syngas yield (b) in long-term stability tests at 550 °C of bimetallic Pd (1)-Ni(0.5)/CeO_2/IWI (blue) and Pd (1)-Ni(0.5)/CeO_2/BM (red) catalysts, and monometallic Pd (1)/CeO_2/BM (black). GHSV = 12 × 10^3 h^{-1}, F/W = 60 L h^{-1} g^{-1}. Raman spectra recorded on these catalysts after the stability test (c). (For interpretation of the references to color/colour in this figure legend, the reader is referred to the Web version of this article.)

methods were analyzed. For comparative purposes, monometallic Pd/CeO_2 catalyst prepared by BM with 1 wt% Pd was also tested. Fig. 10a and b shows the methane conversion and yield of syngas, respectively. As expected, both the initial methane conversion and syngas yield of the bimetallic catalysts were significantly higher than those of the monometallic sample, and the Pd–Ni/CeO_2/BM catalyst performed better than Pd–Ni/CeO_2/IWI. More interestingly, the catalytic performance of the three samples showed a constant decrease of the methane conversion rate of ~0.32% h^{-1} and ~0.37% h^{-1} for the bimetallic catalysts prepared by BM and IWI methods, respectively, and ~0.32% h^{-1} for the monometallic sample up to the first 40 h on stream. However, after 40 h, the catalytic performance of the bimetallic catalyst prepared by BM reached a steady state (in both methane conversion and syngas production) and the deactivation rate was practically zero (0.01% h^{-1}). In contrast, the deactivation of the bimetallic catalyst prepared by IWI and the monometallic sample Pd/CeO_2/BM did not stop and continued progressing with a similar rate. Then, the bimetallic sample prepared by ball milling not only showed higher methane conversion and syngas production, but also a remarkable higher stability. Fig. 10c shows the Raman spectra of the carbon region for the three samples after the long-term stability test. The spectra show three signals at about ~1200 cm^{-1}, ~1345 cm^{-1} and ~1595 cm^{-1}, which correspond to the second-order longitudinal optical mode (2LO) of CeO_2 and the D and G characteristic bands of carbon, respectively [13,27]. The intensity of the D and G bands of carbon follows the trend Pd–Ni/CeO_2/IWI > Pd/CeO_2/BM >> Pd–Ni/CeO_2/BM, which is exactly the opposite trend of stability. It can be concluded that the higher stability of the bimetallic sample prepared by BM is related to its ability to suppress the deposition of carbon during POM, which again points to the existence of unique active sites in the catalyst originating from an intimate and particular synergy between Pd and Ni on CeO_2 thanks to ball milling.

Conclusions

In summary, CeO_2-supported monometallic Pd and Ni and bimetallic Pd–Ni catalysts were prepared by ball milling (BM) and by conventional impregnation (IWI) and were characterized and tested to produce syngas using the POM process at 300–550 °C. The catalytic results revealed that methane conversion and syngas yield followed the order Pd–Ni/CeO_2/BM > Pd–Ni/CeO_2/IWI >> Pd/CeO_2/BM > Pd/CeO_2/IWI >> Ni/CeO_2/BM > Ni/CeO_2/IWI >> CeO_2. A strong synergy between Pd and Ni on CeO_2 occurs in the bimetallic samples prepared by BM, resulting in much more active sites for POM, particularly at low temperature (450 °C). Raman spectroscopy, HRTEM-EDX, XPS and H_2-TPR point to an extremely high dispersion of Pd and Ni in Pd–Ni/CeO_2/BM. Importantly, the Pd–Ni/CeO_2 bimetallic catalysts prepared by BM not only produced syngas at lower temperature compared to the bimetallic catalysts prepared by IWI, but also showed higher catalytic stability in long-term experiments (100 h on stream at 550 °C). This was related to less carbon deposition.

Another important conclusion of this work was obtained by studying the effect of Pd and Ni loadings in the bimetallic

Pd–Ni/CeO_2 catalysts prepared by BM and IWI. A series of bimetallic catalysts were prepared by keeping a total metal loading of 1.5 wt% and varying the Pd amount between 0.016 and 1 wt%. Whereas methane conversion increased gradually with the Pd content for the Pd–Ni/CeO_2/IWI catalysts, it was maintained approximately constant for the Pd–Ni/CeO_2/BM samples, with maximum methane conversion and syngas yield values for Pd (0.12)-Ni(1.38)/CeO_2/BM. This means that highly active catalysts for POM can be designed by properly ball milling small amounts of Pd with Ni. The best ball milling parameters were 50 Hz and 20 min (BPR = 10.2).

Declaration of competing interest

The authors declare that they have no known competing financial interests or personal relationships that could have appeared to influence the work reported in this paper.

Acknowledgements

This work was supported by projects MICINN/FEDER PID2021-124572OB-C31 and GC 2017 SGR 128. SF is grateful to Generalitat de Catalunya for PhD grant 2019 FI_B 00908. XV is grateful to Spanish Government, Ministerio de Ciencia, Innovación y Universidades Juan de la Cierva-Incorporación program for an individual fellowship grant agreement IJCI-2017-31449. JL is a Serra Húnter Fellow and is grateful to ICREA Academia program.

REFERENCES

[1] Li B, et al. *Synthesis gas production from partial oxidation of methane over highly dispersed Pd/SiO_2 catalyst*. Fuel 2013;103:1032–8.
[2] Yabe T, Sekine Y. Methane conversion using carbon dioxide as an oxidizing agent: a review. Fuel Process Technol 2018;181:187–98.
[3] Lunsford JH. Catalytic conversion of methane to more useful chemicals and fuels: a challenge for the 21st century. Catal Today 2000;63(2–4):165–74.
[4] York AP, Xiao T, Green ML. Brief overview of the partial oxidation of methane to synthesis gas. Top Catal 2003;22(3):345–58.
[5] Fleys M, et al. *Investigation of the reaction of partial oxidation of methane over Ni/La_2O_3 catalyst*. Energy Fuels 2006;20(6):2321–9.
[6] Abdulrasheed A, et al. A review on catalyst development for dry reforming of methane to syngas: recent advances. Renew Sustain Energy Rev 2019;108:175–93.
[7] Ryu J-H, et al. Promotion of palladium-based catalysts on metal monolith for partial oxidation of methane to syngas. Appl Catal B Environ 2008;80(3–4):306–12.
[8] Bhattacharya A, et al. Selective oxidation of methane to carbon monoxide on supported palladium catalyst. Appl Catal Gen 1992;80(1):L1–5.
[9] Singha RK, et al. *Synthesis effects on activity and stability of Pt-CeO_2 catalysts for partial oxidation of methane*. Mol Catal 2017;432:131–43.
[10] Kaddeche D, Djaidja A, Barama A. Partial oxidation of methane on co-precipitated Ni–Mg/Al catalysts modified with copper or iron. Int J Hydrogen Energy 2017;42(22):15002–9.
[11] Cumming L, et al. Researching candidate sites for a carbon storage complex in the Central Appalachian Basin, USA. Int J Greenh Gas Control 2019;88:168–81.
[12] Hu YH, Ruckenstein E. *Catalytic conversion of methane to synthesis gas by partial oxidation and CO_2 reforming*. ChemInform 2004;35(49):297–345.
[13] Fazlikeshteli S, Vendrell X, Llorca J. *Low-temperature methane partial Oxidation over Pd Supported on CeO_2: Effect of the preparation Method and precursors*. Reactions 2021;2(1):30–42.
[14] Zaman J. Oxidative processes in natural gas conversion. Fuel Process Technol 1999;58(2–3):61–81.
[15] Koh AC, et al. Hydrogen or synthesis gas production via the partial oxidation of methane over supported nickel–cobalt catalysts. Int J Hydrogen Energy 2007;32(6):725–30.
[16] Enger BC, Lødeng R, Holmen A. A review of catalytic partial oxidation of methane to synthesis gas with emphasis on reaction mechanisms over transition metal catalysts. Appl Catal Gen 2008;346(1–2):1–27.
[17] Rostrup-Nielsen JR. Fuels and energy for the future: the role of catalysis. Catal Rev 2004;46(3–4):247–70.
[18] Colussi S, et al. Nanofaceted Pd-O sites in Pd-Ce surface superstructures: enhanced activity in catalytic combustion of methane. Angew Chem Int Ed 2009;48(45):8481–4.
[19] Fouladvand S, et al. Methane oxidation over Pd supported on ceria–alumina under rich/lean cycling conditions. Top Catal 2013;56(1–8):410–5.
[20] Matam SK, et al. *Revisiting the problem of active sites for methane combustion on Pd/Al_2O_3 by operando XANES in a lab-scale fixed-bed reactor*. J Phys Chem C 2010;114(20):9439–43.
[21] Mattos LV, et al. *Partial oxidation of methane on Pt/Ce–ZrO_2 catalysts*. Catal Today 2002;77(3):245–56.
[22] Luo Z, et al. *TiO_2 Supported gold–palladium catalyst for effective syngas production from methane partial oxidation*. Appl Catal Gen 2018;554:54–63.
[23] Ramírez-López R, Elizalde-Martinez I, Balderas-Tapia L. *Complete catalytic oxidation of methane over Pd/CeO_2–Al_2O_3: The influence of different ceria loading*. Catal Today 2010;150(3–4):358–62.
[24] Stolle A. Technical implications of organic syntheses in ball mills. Ball milling towards green synthesis: applications, projects, challenges 2014;7(31):241.
[25] Moosakazemi F, et al. Effect of design and operational parameters on particle morphology in ball mills. Int J Miner Process 2017;165:41–9.
[26] Piras CC, Fernández-Prieto S, De Borggraeve WM. Ball milling: a green technology for the preparation and functionalisation of nanocellulose derivatives. Nanoscale Adv 2019;1(3):937–47.
[27] Wu Z, et al. *Probing defect sites on CeO_2 nanocrystals with well-defined surface planes by Raman spectroscopy and O_2 adsorption*. Langmuir 2010;26(21):16595–606.
[28] Carter JC, et al. *Raman spectroscopic evidence supporting the existence of $Ni_4(OH)_4^{4+}$ in aqueous, $Ni(NO_3)_2$ solutions*. Anal Chim Acta 2004;514(2):241–5.
[29] Lucentini I, et al. *Ammonia decomposition over 3D-printed CeO_2 structures loaded with Ni*. Appl Catal Gen 2020;591:117382.
[30] Weber W, Hass K, McBride J. *Raman study of CeO_2: second-order scattering, lattice dynamics, and particle-size effects*. Phys Rev B 1993;48(1):178.
[31] Danielis M, et al. Outstanding methane oxidation performance of palladium-embedded ceria catalysts prepared by a one-step dry ball-milling method. Angew Chem 2018;130(32):10369–73.
[32] Pang J, et al. *Mesoporous Cu_2O–CeO_2 composite nanospheres with enhanced catalytic activity for 4-nitrophenol reduction*. Appl Surf Sci 2018;439:420–9.

[33] Molinari M, et al. Water adsorption and its effect on the stability of low index stoichiometric and reduced surfaces of ceria. J Phys Chem C 2012;116(12):7073–82.
[34] Rynkowski JM, et al. *Characterization of Ru/CeO_2-Al_2O_3 catalysts and their performance in CO2 methanation*. React Kinet Catal Lett 2000;71(1):55–64.
[35] Mierczynski P, et al. *High active and selective Ni/CeO_2–Al_2O_3 and Pd–Ni/CeO_2–Al_2O_3 catalysts for oxy-steam reforming of methanol*. Catalysts 2018;8(9):380.
[36] Kugai J, et al. *Effects of nanocrystalline CeO_2 supports on the properties and performance of Ni–Rh bimetallic catalyst for oxidative steam reforming of ethanol*. J Catal 2006;238(2):430–40.
[37] Tanksale A, et al. Effect of Pt and Pd promoter on Ni supported catalysts—a TPR/TPO/TPD and microcalorimetry study. J Catal 2008;258(2):366–77.
[38] Rynkowski J, Paryjczak T, Lenik M. *On the nature of oxidic nickel phases in NiO/γ-Al_2O_3 catalysts*. Appl Catal Gen 1993;106(1):73–82.
[39] Mierczynski P, Maniukiewicz W, Maniecki TP. *Comparative studies of Pd, Ru, Ni, Cu/$ZnAl_2O_4$ catalysts for the water gas shift reaction*. Cent Eur J Chem 2013;11(6):912–9.
[40] Luo M-F, et al. *Characterization study of CeO_2 supported Pd catalyst for low-temperature carbon monoxide oxidation*. Catal Lett 1998;50(3):205–9.
[41] Jen H-W, et al. Characterization of model automotive exhaust catalysts: Pd on ceria and ceria–zirconia supports. Catal Today 1999;50(2):309–28.
[42] York AP, Xiao T, Green ML. Brief overview of the partial oxidation of methane to synthesis gas. Top Catal 2003;22(3–4):345–58.
[43] Deutschmann O, Schmidt LD. Modeling the partial oxidation of methane in a short-contact-time reactor. AIChE J 1998;44(11):2465–77.
[44] Tavazzi I, Beretta A, Groppi G, Forzatti P. *Development of a molecular kinetic scheme for methane partial oxidation over a Rh/α-Al_2O_3 catalyst*. J Catal 2006;241(1):1–13.
[45] Chen Y, et al. A straightforward method to prepare supported Au clusters by mechanochemistry and its application in photocatalysis. Appl Mater Today 2020;21:100873.
[46] Leitenburg C. *A novel and simple route to catalysts with a high oxygen storage capacity: the direct room-temperature synthesis of CeO_2–ZrO_2 solid solutions*. J Chem Soc, Chem Commun 1995;(21):2181–2.
[47] Senftle TP, Van Duin AC, Janik MJ. Role of site Stability in methane Activation on PdxCe1–xOδ surfaces. ACS Catal 2015;5(10):6187–99.
[48] Senftle TP, Van Duin AC, Janik MJ. Methane activation at the Pd/CeO2 interface. ACS Catal 2017;7(1):327–32.
[49] Han Z, et al. Propane dehydrogenation over Pt–Cu bimetallic catalysts: the nature of coke deposition and the role of copper. Nanoscale 2014;6(17):10000–8.
[50] Chen Y, Chen J. *Selective hydrogenation of acetylene on SiO_2 supported Ni-In bimetallic catalysts: Promotional effect of in*. Appl Surf Sci 2016;387:16–27.